BMB
Reports

Invited Mini Review

Two-photon probes for biomedical applications

*Chang Su Lim & Bong Rae Cho**
Department of Chemistry, Korea University, Seoul 136-701, Korea

Two-photon microscopy (TPM), which uses two photons of lower energy as the excitation source, is a vital tool in biology and clinical science, due to its capacity to image deep inside intact tissues for a long period of time. To make TPM a more versatile tool in biomedical research, we have developed a variety of two-photon probes for specific applications. In this mini review, we will briefly discuss two-photon probes for lipid rafts, lysosomes, mitochondria, and pH, and their biomedical applications. [BMB Reports 2013; 46(4): 188-194]

INTRODUCTION

Optical imaging with fluorescence microscopy is a vital tool in the study of living systems. The most common method for cell imaging is confocal microscopy, which utilizes the fluorescence emitted from probe-labeled cells, by excitation with a single UV-Vis photon (1). Two-photon microscopy (TPM) is an advanced version of confocal microscopy, which utilizes two near-infrared (NIR, 700-1,100 nm) photons as the excitation source (2, 3). With the advent of commercial TPM, this new technique has become an indispensable tool in biology and clinical science, due to the advantages it offers. Compared with the UV-Vis photons used in confocal microscopy, the NIR light photons used by TPM can penetrate deeper inside tissues, with little self-absorption. This allows imaging deep inside a live tissue, with minimum interference from auto-fluorescence and tissue preparation artifacts, which can extend as much as 70 μm from the tissue surface. Second, two-photon (TP) excitation is intrinsically localized, and can provide higher spatial resolution. This enables researchers to obtain hundreds of sectional images of a thick tissue sample, along the z-direction. Third, the total energy absorbed by the tissue sample from the femtosecond pulse laser is much lower, than that from the continuous wave laser used in confocal microscopy. This minimizes the photobleaching of the probes, and photodamage of the biological samples. To make TPM a more versatile tool in biology and medicine, researchers need a wider variety of TP probes, for specific applications. However, progress in this field is hindered by the lack of efficient TP probes. We have proposed a guideline for the design of a useful TP probe; it should have high selectivity for the biological targets, appreciable water solubility and cell permeability to stain the cells, and significant TP action cross section (a measure of TP excited fluorescence (TPEF) intensity emitted from the probe), to obtain bright TPM image, high photostability and low toxicity for long term imaging (4). In this context, we have developed a variety of TP probes for lipid rafts (5-8), lysosomes (9-11), mitochondria (11), pH (10, 12), metal ions (Ca^{2+}, Mg^{2+}, Zn^{2+}, Cu^{2+}, Cu^{+}, Na^{+}, Hg^{2+}, Ni^{2+}) (13, 14), reactive oxygen species (ROS) (15, 16), reactive nitrogen species (RNS) (17), thiols (18, 19), hydrogen sulfide (20), and glucose (21, 22), which meet all of the requirements mentioned above. In this mini review, we will briefly discuss the TP probes for lipid rafts, lysosomes, mitochondria, and pH that were developed in our laboratory, and their biomedical applications.

Two-photon probes for membrane. Visualization of lipid rafts by TPM

One of the most important controversies in cell biology is the lipid raft hypothesis (23, 24). To visualize such domains in the cell, laurdan has been extensively used as the polarity probe, because it accurately reflects the rigid and fluid domains in giant unilamellar vesicles (GUVs) composed of 1,2-dipalmitoyl-*sn*-glycero-3-phosphocholine (DPPC) (25). Unfortunately, however, it does not behave as well in cells. In fact, some of the literature results obtained with laurdan-labeled cells are hard to reproduce (26). To find the origin of this problem, we have conducted an extensive photophysical study on laurdan (5). The fluorescence spectra of laurdan showed gradual bathochromic shifts, with a solvent polarity increase in the order c-Hex < DMF < EtOH, but a blue shift in water. Interestingly, the fluorescence spectrum of laurdan in aqueous medium has never been reported. In DPPC, laurdan showed an emission maximum at 440 nm, whereas in 1,2-di-oleoyl-*sn*-glycero-3-phosphocholine (DOPC) it showed a broad spectrum that could be dissected into two bands centered at 439 and 484 nm, respectively. The emission spectra of laurdan in DOPC/sphingomyelin/cholesterol (1 : 1 : 1, raft mixture) and DPPC showed reasonable overlap, indicating that this probe preferentially reflects the gel domain, compared to the fluid domain, in the raft mixture. All of these results have been at-

*Corresponding author. Tel: +82-2-3290-9129; Fax: +82-2-3290-3544; E-mail: chobr@korea.ac.kr
http://dx.doi.org/10.5483/BMBRep.2013.46.4.045

Received 22 February 2013

Keywords: Autophagy, Lipid rafts, Two-photon probes

ISSN: 1976-6696 (print edition) / 1976-670X (electronic edition)

tributed to the negligible solubility of laurdan in water. Since laurdan exists as aggregates in water, the fluorescence is weak and blue-shifted. In GUVs composed of DPPC, laurdan behaves ideally, regardless of the rigidity of the GUVs, presumably because it is aligned parallel to the DPPC by the favorable hydrophobic interactions between the saturated hydrocarbon tails in both molecules. On the other hand, such interactions do not exist between laurdan and DOPC, which has *cis*-double bonds in the tail. That is why laurdan exists as free form, and aggregates in DOPC to result in a broad spectrum. In raft mixture, which is a good model for the cell membrane, laurdan is preferentially located near DPPC, and shows a spectrum similar to that in DPPC. These results confirm that laurdan cannot accurately reflect the rigid and fluid domains in the cell membrane. Indeed, the generalized polarization (GP, the value ranges from 0.0 to 1.0, such that the larger number indicates a more hydrophobic environment) curve of the laurdan-labeled cells was skewed toward the high GP region (figure not shown). Moreover, the high GP curve showed little change upon treatment with MβCD, a lipid-raft-destroying reagent that acts by removing cholesterol from the plasma membrane.

To visualize the lipid rafts without the above mentioned problems, we have developed C-laurdan (CL), by introducing a carboxylic acid moiety at the nitrogen atom of laurdan (5, 6). It was expected that the carboxylic acid head group would im-

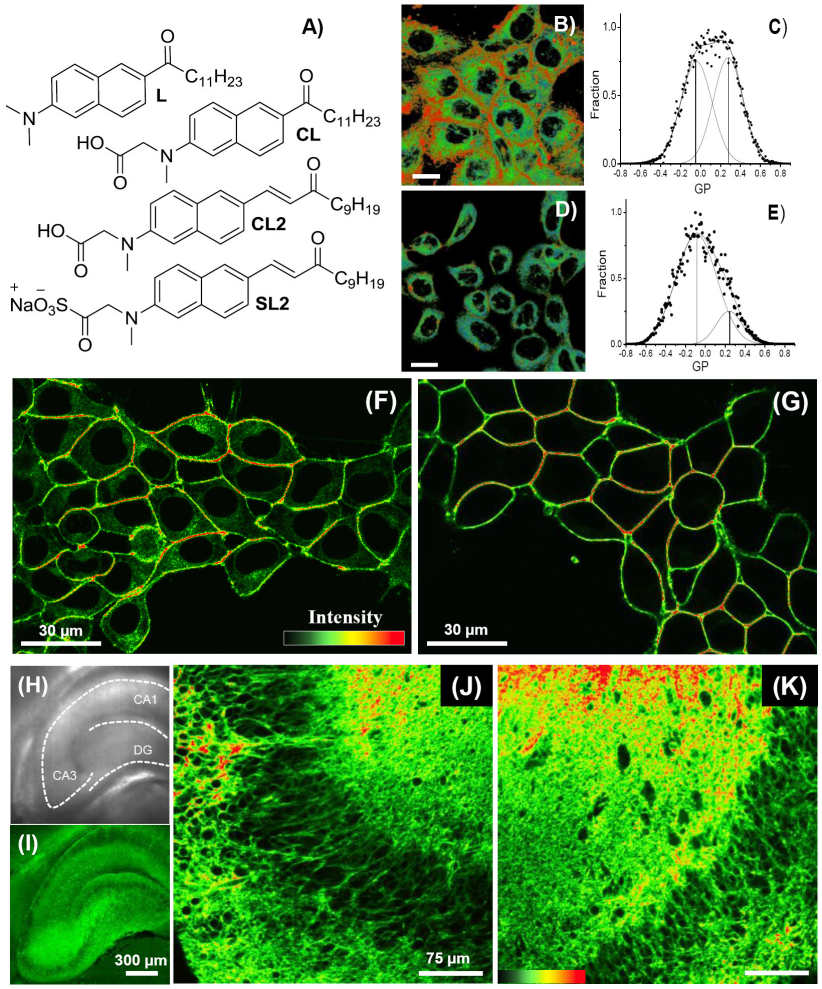

Fig. 1. (A) Structures of laurdan (L), CL, CL2, and SL2. (B, D) GP images of the C-laurdan-labeled A431 cells (B) before, and (D) after treatment with MβCD and (C, E) GP distribution curves. Scale bars = 10 μm. (F, G) Pseudocolored TPM images of (F) CL2- and (G) SL2-labeled 293T cells. (H-K) Images of a fresh rat hippocampal slice with 10 μm SL2. (H) Bright-field image and (I) TPM image of the CA1 and CA3 regions, as well as the dentate gyrus (DG), by 10× magnification. Twenty-five TPM images were accumulated along the z-direction at a depth of ~100-200 μm. (J, K) Pseudocolored TPM image of the (J) CA3, and (K) DG layer at a depth of ~100 μm by 40× magnification. The TPM images were collected at 410-530 nm, upon excitation at 800 nm with femtosecond pulses.

prove the water solubility to avoid aggregation, and enhance the hydrophilic interactions between the carboxylates and lipid head groups. This would help CL align parallel to the lipid molecules in the GUVs and cell membrane, regardless of whether the lipid hydrocarbon tails are saturated or unsaturated. These expectations were borne out by the experiments. In contrast to laurdan, the fluorescence spectra of CL showed gradual bathochromic shifts in the order c-Hex < DMF < EtOH < H_2O, and discrete emission maxima at 442 and 486 nm in the GUVs composed of DPPC and DOPC, respectively. In the raft mixture, the emission spectrum was almost the same as the sum of the spectra in DPPC and DOPC, indicating that CL can accurately represent the rigid and fluid domains in the GUVs. Moreover, CL exhibited larger TP action cross section than laurdan, to result in a brighter TPM image of the cells when labeled with CL. Further, the GP curve of the CL-labeled cell was symmetrical, and could be deconvoluted into two curves of similar shape and area (Fig. 1B, C). When the cells were treated with MβCD, the higher GP curve decreased dramatically, without appreciable change in the lower one (Fig. 1D, E). These results demonstrated that CL is a useful polarity probe, which can accurately represents lipid rafts and non-rafts in the cell membrane. The utility of CL in cell biology has been demonstrated by other groups (27-32).

A major drawback of a polarity probe such as CL is the uncertainties involved in the calculation of the GP values, which requires the measurements of the emission intensities in the short and long wavelength regions, and the G value (the sensitivity correction factor for the two different wavelength ranges). To overcome this problem, we have developed a TP turn-on probe (CL2), which emits TPEF only in the lipid rafts (7). Compared to CL, CL2 showed larger bathochromic shifts, and sharper decrease in the fluorescence intensity in a more polar solvent. The relative fluorescence intensity of CL2 in DPPC/raft mixture/DOPC was 8.4/7.4/1.0. This allowed direct visualization by TPM of the lipid rafts against the dim background, due to the fluid domain. Indeed, the TPM image of the macrophase labeled with CL2 showed a bright region (red color) (Fig. 1F), which disappeared upon treatment with MβCD, returned to near the base level when treated with excess cholesterol, and overlapped well with the OP image of BODIPY-GM1, a well-known OP fluorescent probe for lipid rafts (figures not shown). These results demonstrate the utility of CL2 as the TP turn-on probe for the lipid rafts.

Although CL2 is an excellent TP turn-on probe, it has one shortcoming. It internalizes into the cytoplasm, upon prolonged incubation with cells (Fig. 1F). To overcome this problem, we have developed a TP turn-on probe having a sulfonate group, in place of the carboxylic acid moiety in the CL2, with the expectation that the more hydrophilic sulfonate head group would minimize the internalization (8). As expected, the photophysical properties of SL2 were very similar to those of CL2, both in solution and GUVs, with dramatic decrease in the TPEF intensity in more polar environment. The TPM image of the SL2-labeled 293T cell revealed a bright domain in the plasma membrane, which disappeared upon treatment with MβCD, returned to near the base level when treated with excess cholesterol, and overlapped well with the OP image of fluorescent cholera toxin B (CTB), a well-known protein that induces the formation of larger raft domains, and BODIPY-GM1, a commercial OP fluorescence probe for lipid rafts (figures not shown). Noteworthy was the minimum internalization of SL2 into the cytoplasm (Fig. 1G). We further demonstrated the utility of SL2 in tissue imaging. The bright field image of a part of fresh hippocampal slices from postnatal three-day-old rats reveals the CA1 and CA3 regions, as well as the dentate gyrus (Fig. 1H). The TPM images of the SL2-labled tissue slice taken at higher magnifications clearly resolved the distribution of the lipid rafts in the pyramidal neuron layer of the CA1 and dentate gyrus regions (Fig. 1J and K). These results establish the utility of SL2 as the TP turn-on probe for the lipid rafts.

Two-photon probes for lysosomes and mitochondria. Visualization of autophagy by TPM

Lysosomes are acidic organelles that are used to digest food, or break down the cells when they die (33). To detect lysosomes by TPM, we have developed TP lysotrackers, which emit TPEF in the short (CLT-blue) and long (CLT-yellow) wavelength regions (9). The emission maxima and the TP action cross sections of CLT-blue and CLT-green are 470 and 550 nm, and 50 and 47 GM, respectively. To assess whether CLT-blue and CLT-green can detect lysosomes in live cells, we performed co-localization experiments. The TPM image of CLT-blue-labeled cells overlapped well with the OPM image of the lysosomes (Fig. 2A-C), but not with those of Golgi apparatus and mitochondria (figure not shown). A similar result was observed with CLT-green, demonstrating the utilities of CLT-blue and CLT-yellow as TP lysotrackers (figure not shown). Moreover, the TPM images of HeLa cells colabeled with CLT-blue and CLT-yellow showed almost perfect overlap. This outcome can be attributed to two factors. First, the two TPM images are obtained simultaneously, whereas the TPM and OPM images are obtained one after another, with interval during which the lysosomes can move. Second, the two TPM images compare the lysosomal distribution in the same x-y plane, whereas OPM images reveal those in the entire depth of the cell. These results demonstrate the advantage of using two TP probes in the colocalization experiments.

Mitochondria are vital organelle that exists in most eukaryotic cells (34). Mitochondria provide the energy of the cell, and are involved in many biological processes, such as signaling, cellular differentiation, cell death, and cell growth (35). Along with lysosomes, mitochondria play key roles in autophagy, a process to relocate the nutrients, which are generated by degrading old, damaged or surplus mitochondria through lysosomes, from unnecessary processes to more essential processes. To visualize autophagy by TPM, we have devel-

oped TP probes for lysosomes and mitochondria, which emit TPEF in the short (BLT-blue, λ= 469 nm) and long wavelength regions (FMT-green, λ= 572 nm) (11).

The TP action cross-sections of BLT-blue and FMT-green are 160 and 175 GM, respectively, at 750 nm. These values predict bright TPM images of the cells when labeled with these probes. The TPM image of RAW 264.7 cells stained with BLT-blue and FMT-green matched well with the OPM images of lysosome and mitochondria (Fig. 2G-L), but not with those of other organelles. Also, BLT-blue and FMT-green are insensitive to the pH value in the biologically relevant pH range, and exhibit high photostability and low cytotoxicity. These results demonstrate that BLT-blue and FMT-green can detect lysosomes and mitochondria, respectively, by TPM for a long period of time, with minimum interference from pH or cytotoxicity.

We then tested the abilities of BLT-blue and FMT-green to visualize autophagy, by dual-color imaging. Autophagy proceeds by enclosing a portion of cytoplasm, including mitochondria, in a phagophore or isolation membrane, to form

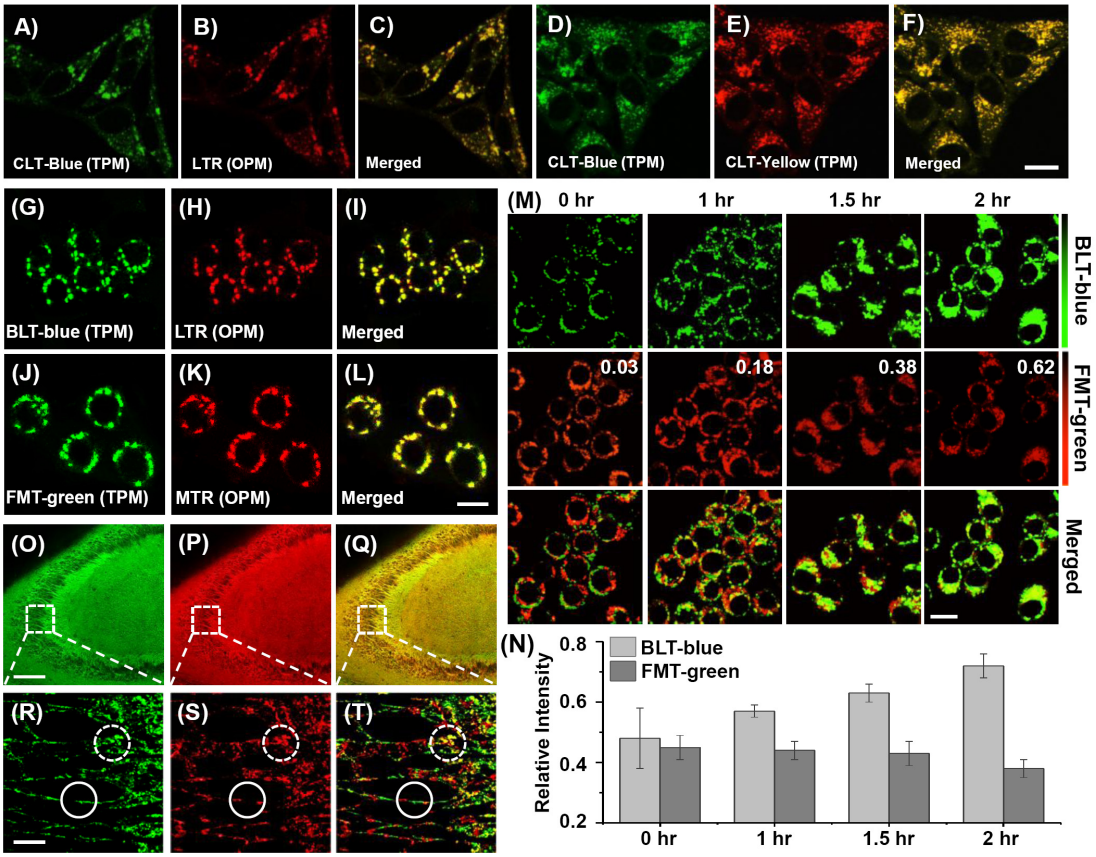

Fig. 2. OPM, TPM, and merged images of HeLa cells colabeled with (A-F) CLT-blue (2 μM), LTR (1 μM), and CLT-yellow (2 μM) respectively. The excitation wavelengths were 543 (LTR), 750 (CLT-blue), and 840 nm (CLT-yellow), the OP fluorescence was collected at 580-700 nm (LTR), and TPEF was collected at 400-520 (CLT-blue) and 550-625 nm (CLT-yellow). (D, E) For colocalization between CLT-blue and CLT-yellow, the probes were excited at 750 nm and the TPEF was recorded at 400-475 (CLT-blue) and 550-625 nm (CLT-yellow), respectively. Areas of colocalization appear in orange-red. (G, J) TPM and (H, K) OPM images of Raw 264.7 cells co-labeled with (G, H) BLT-blue and LTR, and (J, K) FMT-green and MTR. (I, L) Merged images. Dual-color TPM images of Raw 264.7 cells co-labeled with (M: top column) BLT-blue and (M: middle column) FMT-green. (M: bottom column) Merged images. (M) The cells were treated with rapamycin (50 μg/ml) for 0-2 hr to induce autophagy. The numbers in the middle column are the co-localization coefficients (A value) of the red with the green domains. (N) Relative TPEF intensities of the probe-labeled cells. Dual-channel TPM images of a rat hippocampal slice co-labeled with BLT-blue and FMT-green collected at a depth of about 120 μm by O-Q) 10× and R-T) 200× magnification, respectively. (Q, T) Merged images. (R-T) The images in the white solid circles clearly resolved lysosomes and mitochondria, and showed little overlap with A value of 0.17 (T), whereas those in the white-dotted circles (R-T) showed partial overlap with A value of 0.41 (T). The TPM images were collected at (G, M): top column, (O, R): λ = 400-450 (BLT-blue); (J, M): middle column, (P, S): 550-600 nm (FMT-green) and OPM images were collected at (H): λ = 580-650 (LTR), (K): 630-680 nm (MTR), respectively. The wavelengths for one- and two-photon excitation were λ = 543 and 750 nm, respectively. Cells shown are representative images from replicate experiments (n = 5). Scale bars: (F) 20, (L, M, R) 15, and (O) 300 μm.

an autophagosome. The outer membrane of the autophagosome fuses with endosome, and then with lysosome, and the contents are degraded (34, 36, 37). The TPM images of the RAW 264.7 cells co-labeled with BLT-blue and FMT-green revealed lysosomes (green spots) and mitochondria (red spots; Fig. 2M; 0 hr). When the cells were treated with rapamycin (50 μg/ml), a pharmacologic agent that induces autophagy (37), the TPEF intensity increased at 400-450 nm, and decreased at 550-600 nm (Fig. 2M: 2 h). This outcome indicates the activation of lysosomes and breakdown of mitochondria, a result consistent with autophagy. After 1 h, the green and red domains began to merge, as revealed by the appearance of the yellow regions (Fig. 2M: 1 h). The Pearson's co-localization coefficient (*A*), which describes the correlation of the intensity distribution between the channels (13) of the red with the green domain, increased from 0.03 to 0.18 to 0.38 to 0.62, after starvation for 0, 1, 1.5, and 2 h, respectively. This result indicates the progress of the fusion between autophagosoms and lysosomes during the autophagy. When the cells were starved in an amino acid/serum-deprived buffer, the lysosomal activity increased with concomitant degradation of mitochondria, and gradual increase in the fusion between them (figures not shown). These results establish that BLT-blue and FMT-green can monitor the autophagy in live cells by dual-color imaging, by using a single excitation source.

We further investigated the utility of BLT-blue and FMT-green in tissue imaging. The TPM images obtained by collecting the signals at short and long wavelengths, and the merged image, revealed the distribution of the lysosome and mitochondria at a depth of 120 μm (Fig. 2O-Q).

The TPM images taken at a higher magnification clearly resolved the distribution of the two organelles in the pyramidal neuron layer of the CA3 region (Fig. 2R-T). Moreover, the two images in the white solid circles showed little overlap (Fig. 2R-T). These results demonstrate that BLT-blue and FMT-green can detect the two organelles, with minimum interference from each other, at 120 μm depth in live tissues, by using TPM.

A ratiometric two-photon probe for pH. Measurement of pH in human tissue by TPM

Gastroesophageal reflux disease (GERD) is a common disease associated with the pH change in the esophageal lumen, caused by the reflux of acidic gastric contents from the stomach (38). There is an interesting hypothesis that, as the refluxed acid infiltrates into the widened intercellular spaces and weakened cell junctions in the esophagus and stimulates the nociceptor, it thereby causes GERD-related symptoms (39). Approximately 70% of the GERD-related patients are endoscopy negative, which is called nonerosive reflux disease

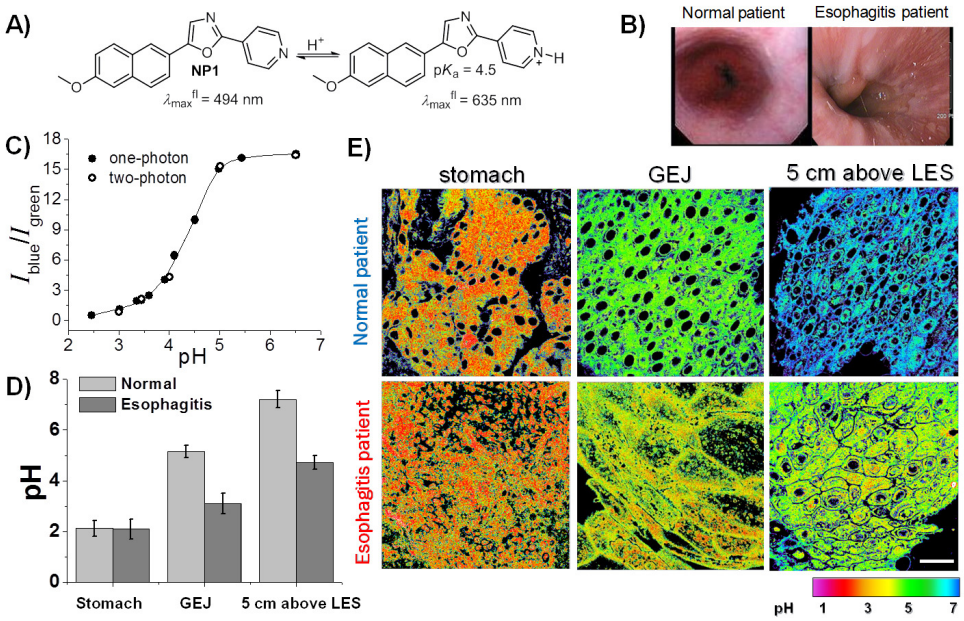

Fig. 3. (A) Equilibrium between NP1 and $NP1H^+$. (B) Endoscope images of control and esophagitis patients. (C) Plots of I_{blue}/I_{green} versus pH as determined by one- (●) and two-photon mode (○) microscopy. Blue = 400-500 nm; green = 600-750 nm. The solid line is the theoretically fitted curve. (D) The average and standard deviation of the pH values that were estimated from the I_{blue}/I_{green} ratios and fluorescence titration curve. (E) Ratiometric TPM images of stomach and esophagitis tissues labeled with 20 μM NP1 for 1 h. Images were acquired by using 740 nm excitation and fluorescent emission windows at: blue = 400-475 nm, green = 550-650 nm. The images shown are the representative images obtained at a depth of 120 μm (n=7). Scale bar: 30 μm.

(NERD). However, there is no gold standard for the diagnosis of NERD (40, 41). To quantitatively measure the pH in the human tissue, and possibly diagnose NERD, we have developed a ratiometric TP probe for pH (NP1) (12).

NP1 emitted strong fluorescence at 500 nm, which decreased gradually, with concomitant increase at 670 nm as the pH decreased (Fig. 3C), presumably because of the protonation at the pyridyl nitrogen atom (Fig. 3A). The emission intensity ratios (I_{blue}/I_{green}; blue = 400-500 nm, green = 600-750 nm) increased by 12-fold (Fig. 3C), as the pH was changed from 2.45 to 6.50. Moreover, the I_{blue}/I_{green} ratio determined by the TP mode fitted well on the OP titration curve (Fig. 3C). Further, the TP action cross-section value of NP1 was 155 GM at 740 nm, which allowed us to obtain bright TPM images of the cells and human tissues that were labeled with NP1 (see below). These results establish that NP1 can serve as a ratiometric TP probe that can estimate the pH value in a TP mode.

We then tested the ability of NP1 to measure the pH in human tissues. The I_{blue}/I_{green} ratios were obtained from the TPM images of the NP1-labeled tissues, at the depths of 90-180 μm. The pH values were then estimated from the I_{blue}/I_{green} ratios, and the titration curve. The results show that the pH value in the stomach is approximately 2.1, and is almost the same for the normal and esophagitis patients, respectively (Fig. 3C, E). On the other hand, the pH values measured at the gastro-esophageal junction (GEJ) and 5 cm above the proximal border of the lower esophageal sphincter (LES) are significantly lower for esophagitis patients than in control patients, with pH values of (3.1 ± 0.4) and (4.7 ± 0.5) versus (5.1 ± 0.3) and (7.2 ± 0.3), respectively (Fig. 3D, E). This outcome is consistent with the proposal that the GERD is associated with a decrease in the pH in the esophageal lumen. Further, the ratiometric TPM images obtained at different depths reveal that the textures change slightly, without appreciable differences in the pH value (figure not shown). Therefore, NP1 is clearly capable of measuring the pH in human tissues at depths of 90-180 μm, by using TPM.

CONCLUSIONS

In this review, we summarized the photophysical properties and biomedical applications of a few TP probes that we have developed. We showed that CL is an efficient TP polarity probe, which can accurately represent lipid rafts and non-rafts in the cell membrane, while CL2 and SL2 are useful TP turn-on probes, with which one can visualize lipid rafts as bright domains against dim backgrounds, due to the fluid domains. SL2 is particularly useful for long term imaging, as it shows minimum internalization. We also presented the utility of using two TP probes with different emission wavelengths; dual color TPM imaging is convenient, not only for the colocalization, but also for the visualization of biological processes such as autophagy. We then presented an example of the medical application of a ratiometric TP probe for pH, which can measure the pH deep inside of human tissues, and possibly diagnose NERD. We believe that TPM will further enhance our understanding of biology, when combined with an appropriate TP probe.

Acknowledgements
This work was supported by the Korea Healthcare Technology R&D Project, Ministry of Health & Welfare, Republic of Korea (A111182), and the National Research Foundation grants (No. 2012007850 and 20120005860).

REFERENCES

1. Pawley, J. B. (2006) Handbook of biological confocal microscopy. 3rd ed. Springer, Berlin, Germany.
2. Helmchen, F. and Denk, W. (2005) Deep tissue two-photon microscopy. *Nat. Meth.* **2**, 932-940.
3. Zipfel, W. R., Williams, R. M. and Webb, W. W. (2003) Nonlinear magic: multiphoton microscopy in the biosciences. *Nat. Biotech.* **21**, 1369-1377.
4. Kim, H. M., Fang, X. Z., Yang, P. R., Yi, J. S., Ko, Y. G., Piao, M. J., Chung, Y. D., Park, Y. W., Jeon, S. J. and Cho, B. R. (2007) Design of molecular two-photon probes for in vivo imaging. 2*H*-Benzo[*h*]chromene-2-one *derivatives*. *Tetrahedron Lett.* **48**, 2791-2795.
5. Kim, H. M., Choo, H. J., Jung, S. Y., Ko, Y. G., Park, W. H., Jeon, S. J., Kim, C. H., Joo, T. and Cho, B. R. (2007) A two-photon fluorescent probe for lipid raft imaging: C-Laurdan. *ChemBioChem* **8**, 553-559
6. Kim, H. M., Kim, B. R., Choo, H. J., Ko, Y. G., Jeon, S. J., Kim, C. H., Joo, T. and Cho, B. R. (2008) Two-photon fluorescent probes for biomembrane imaging: Effect of chain length. *ChemBioChem* **9**, 2830-2838.
7. Kim, H. M., Jeong, B. H., Hyon, J. Y., An, M. J., Seo, M. S., Hong, J. H., Lee, K. J., Kim, C. H., Joo, T., Hong, S. C. and Cho, B. R. (2008) Two-photon fluorescent turn-on probe for lipid rafts in live cell and tissue. *J. Am. Chem. Soc.* **130**, 4246-4247.
8. Lim, C. S., Kim, H. J., Lee, J. H., Tian, Y. S., Kim, C. H., Kim, H. M., Joo, T. and Cho, B. R. (2011) A two-photon turn-on probe for lipid rafts with minimum internalization. *ChemBioChem* **12**, 392-395.
9. Son, J. H., Lim, C. S., Han, J. H., Danish, I. A., Kim, H. M. and Cho, B. R. (2011) Two-photon lysotrackers for in vivo imaging. *J. Org. Chem.* **76**, 8113-8116.
10. Kim, H. M., An, M. J., Hong, J. H., Jeong, B. H., Kwon, O., Hyon, J. Y., Hong, S. C., Lee, K. J. and Cho, B. R. (2008) Two-photon fluorescent probes for acidic vesicles in live cells and tissue. *Angew. Chem. Int. Ed.* **47**, 2231-2234.
11. Han, J. H., Park, S. K., Lim, C. S., Park, M. K., Kim, H. J., Kim, H. M. and Cho, B. R. (2012) Simultaneous imaging of mitochondria and lysosomes by using two-photon fluorescent probes. *Chem. Eur. J.* **18**, 15246-15249.
12. Park, H. J., Lim, C. S., Kim, E. S., Han, J. H., Lee, T. H., Chun, H. J. and Cho, B. R. (2012) Measurement of pH values in human tissues by two-photon microscopy. *Angew. Chem. Int. Ed.* **51**, 2673-2676.

13. Kim, H. M. and Cho, B. R. (2009) Two-photon probes for intracellular free metal ions, acidic vesicles, and lipid rafts in live tissues. *Acc. Chem. Res.* **42**, 863-872.
14. Kim, H. M. and Cho, B. R. (2011) Two-photon fluorescent probes for metal ions. *Chem. Asian. J.* **6**, 58-69.
15. Chung, C., Srikun, D., Lim, C. S., Chang. C. J. and Cho, B. R. (2011) A two-photon fluorescent probe for ratiometric imaging of hydrogen peroxide in live tissue. *Chem. Commun.* **47**, 9618-9620.
16. Masanta, G., Heo, C. H., Lim, C. S., Bae, S. K., Cho, B. R. and Kim, H. M. (2012) A mitochondria-localized two-photon fluorescent probe for ratiometric imaging of hydrogen peroxide in live tissue. *Chem. Commun.* **48**, 3518-3520.
17. Seo, E. W., Han, J. H., Heo, C. H., Shin, J. H., Kim, H. M. and Cho, B. R. (2012) A small-molecule two-photon probe for nitric oxide in living tissues. *Chem. Eur. J.* **18**, 12388-12394.
18. Lee, J. H., Lim, C. S., Tian, Y. S., Han, J. H. and Cho, B. R. (2010) A two-photon fluorescent probe for thiols in live cells and tissues. *J. Am. Chem. Soc.* **132**, 1216-1217.
19. Lim, C. S., Masanta, G., Kim, H. J., Han, J. H., Kim, H. M. and Cho, B. R. (2011) Ratiometric detection of mitochondrial thiols with a two-photon fluorescent probe. *J. Am. Chem. Soc.* **133**, 11132-11135.
20. Das, S. K., Lim, C. S., Yang, S. Y., Han, J. H. and Cho, B. R. (2012) A small molecule two-photon probe for hydrogen sulfide in live tissues. *Chem. Commun.* **48**, 8395-8397.
21. Tian, Y. S., Lee, H. Y., Lim, C. S., Park, J., Kim, H. M., Shin, Y. N., Kim, E. S., Jeon, H. J., Park, S. B. and Cho, B. R. (2009) A two-photon tracer for glucose uptake. *Angew. Chem. Int. Ed.* **48**, 8027-8031.
22. Lim, C. S., Chul, C., Kim, H. M., An, M. J., Tian, Y. S., Chun, H. J. and Cho, B. R. (2012) A two-photon turn-on probe for glucose uptake. *Chem. Commun.* **48**, 2122-2124.
23. Leslie, M. (2011) Do lipid rafts exist? *Science* **344**, 1046-1047.
24. Lingwood, D. and Simons, K. (2010) Lipid rafts as a membrane-organizing principle. *Science* **327**, 46-50.
25. Bagatolli, L. A. and Gratton, E. (1999) Two-photon fluorescence microscopy observation of shape changes at the phase transition in phospholipid giant unilamellar vesicles. *Biophys. J.* **77**, 2090-2101.
26. Gaus, K., Gratton, E., Kable, E. P., Jones, A. S., Gelissen, I., Kritharides, L. and Jessup, W. (2003) Visualizing lipid structure and raft domains in living cells with two-photon microscopy. *Proc. Natl. Acad. Sci. U.S.A.* **100**, 15554-15559.
27. Kaiser, H. J., Lingwood, D., Levental, I., Sampaio, J. L., Kalvodova, L., Rajendran, L. and Simins, K. (2009) Order of lipid phases in model and plasma membranes. *Proc. Natl. Acad. Sci. U.S.A.* **106**, 16645-16650.
28. Ekholm, O., Jaikishan, S., Lonnfors, M., Nyholm, T. K. M. and Slotte, J. P. (2011) Membrane bilayer properties of sphingomyelins with amide-linked 2- or 3-hydroxylated fatty acids. *Biochim. Biophys. Acta.* **1808**, 727-732.
29. Yurlova, L., Kahya, N., Aggarwal, S., Kaiser, H. J., Chiantia, S., Bakhti, M., Pewzner, J. Y., Ben, D. O., Futerman, A. H., Brügger, B. and Simons M. (2011) Self-segregation of myelin membrane lipids in model membranes. *Biophys. J.* **101**, 2713-2720.
30. Dodes Traian, M. M., Gonzalez Flecha, F. L. and Levi, V. (2012) Imaging lipid lateral organization in membranes with C-laurdan in a confocal microscope. *J. Lipid. Res.* **53**, 609-616.
31. Klemm, R. W., Ejsing, C. S., Surma, M. A., Kaiser, H. J., Gerl, M. J., Sampaio, J. L., de Robillard, Q., Ferguson, C., Proszynski, T. J., Shevchenko, A. and Simons K. (2009) Segregation of sphingolipids and sterols during formation of secretory vesicles at the trans-Golgi network. *J. Cell. Biol.* **185**, 601-612.
32. Kaiser, H. J., Surma, M. A., Mayer, F., Lecental, I., Grzybek, M., Klemm, R. W., Da Cruz, S., Meisinger, C., Mueller, V., Simons, K. and Lingwood, D. (2011) Molecular convergence of bacterial and eukaryotic surface order. *J. Cell. Biol.* **286**, 40631-40637.
33. Saftig, P. and Klumperman, J. (2009) Lysosome biogenesis and lysosomal membrane proteins: trafficking meets function. *J. Nat. Rev. Mol. Cell Biol.* **10**, 623-635.
34. Levine, B. and Kroemer, G. (2008) Autophagy in the pathogenesis of disease. *Cell* **132**, 27-42.
35. McBride, H. M., Neuspiel, M. and Wasiak, S. (2006) Mitochondria: more than just a powerhouse. *Curr. Biol.* **16**, 551-560.
36. Rodriguez-Enriquez, S., Kim, I. R., Currin, T. and Lemasters, J. J. (2006) Tracker dyes to probe mitochondrial autophagy (mitophagy) in rat hepatocytes. *Autophagy* **2**, 39-46.
37. Singh, S. B., Davis, A. S., Taylor, G. A. and Deretic, V. (2006) Human IRGM induces autophagy to eliminate intracellular mycobacteria. *Science* **313**, 1438-1441.
38. DeVault, K. R. and Castell, D. O. (1999) Updated guidelines for the diagnosis and treatment of gastroesophageal reflux disease. *Am. J. Gastroenterol.* **94**, 1434-1442.
39. Fass, R. and Tougas, G. (2002) Functional heartburn: the stimulus, the pain, and the brain. *Gut* **51**, 885-892.
40. Hershcovici, T. and Fass, R. (2010) An algorithm for diagnosis and treatment of refractory GERD. *Best Pract. Res. Clin. Gastroenterol.* **24**, 923-936.
41. Hershcovici, T. and Fass, R. (2010) Nonerosive reflux disease (NERD). *J. Neurogastroenterol Motil.* **16**, 8-21.